

SeaSonde Radial Velocities: Derivation and Internal Consistency

Belinda Lipa, Bruce Nyden, David S. Ullman, and Eric Terrill

Abstract—This paper describes the methods presently used to produce unaveraged radial velocity maps from radar voltage cross spectra measured by a SeaSonde, including a discussion of the multiple signal classification (MUSIC) algorithm as it is applied to SeaSonde data and methods employed to alleviate difficulties associated with the use of measured antenna patterns. We also describe internal consistency checks including visual observation of the radial velocity map, consideration of the computed uncertainties and quantitative tests of radial velocities measured by two radars along the baseline between the systems. Baseline analysis is illustrated by application to two SeaSonde networks, with contrasting results that lead to a better understanding of SeaSonde output.

Index Terms—Data analysis, high-frequency (HF) radar oceanography, remote sensing.

I. INTRODUCTION

A SEASONDE is a high-frequency (HF) radar system with a compact antenna system consisting of two crossed loops and a monopole that produces maps of the radial component of the ocean surface current velocity. Standard-range SeaSondes typically operate in either the 24–27-MHz or the 12–14-MHz band and long-range SeaSondes in the 4–6-MHz band. For the lower transmit frequency, there is increased range but decreased spatial resolution. Two or more SeaSondes usually operate at separated sites (termed remote sites) to form a network. Radial velocities from the remote sites are combined to give the maps of total current velocity that are probably of greatest interest to users. However, radial velocities and their uncertainties, along with system diagnostics, provide most of the information on data quality, which can be used to evaluate system performance and data analysis procedures.

In this paper, we summarize the methods used by standard SeaSonde software to derive radial current velocities from measured radar cross spectra, including the implementation of the multiple signal classification (MUSIC) algorithm for direction-finding and a discussion of the methods used to incorporate measured antenna patterns. We also outline internal consistency

checks that may be used to assess the quality of the radial velocities. These include visual inspection, evaluation of radial velocity uncertainty estimates, and quantitative tests that can be applied to radial velocities falling along the baseline between two radar sites when it falls over open ocean. These methods are illustrated by application to two specific cases.

The paper is organized as follows. Section II summarizes the methods presently in use to derive radial velocities. Section III describes internal consistency checks for the assessment of the radial velocities. Section IV discusses application of baseline analysis to specific cases. Section V discusses a cause of high baseline deviations: inclusion of noisy spectra in the analysis, which also leads to anomalous total current velocities.

II. DERIVATION OF SEASONDE RADIAL VELOCITIES

Lipa and Barrick [1] described the basic methods for the analysis of broadbeam HF radar Doppler echo spectra to give radial current velocities. In this section, we summarize the analysis procedures presently implemented in the system software to derive radial velocities from SeaSonde radar spectra.

A. Summary of Analysis Procedures

SeaSonde system software performs the following eight steps on the complex voltage time series obtained by the three antennas.

- 1) The complex signal voltages from the three SeaSonde antennas V_i , $i = 1, 2, 3$ for each range cell are combined to give the voltage cross spectra defined by $V_i V_j^*$ where $i, j = 1, 2, 3$. A range cell is a circular annulus defined by the range from the radar and a fixed range increment that is typically 1.5, 3, and 10 km for transmit frequencies in the 24–27-, 12–14-, 4–6-MHz bands, respectively.
- 2) The voltage cross spectra are averaged over a time interval, which is usually set to 10 min for a standard-range SeaSonde (with transmit frequency in either the 12–14-MHz or the 24–27-MHz band) and 30 min for a long-range SeaSonde (transmit frequency in the 4–6-MHz band). The averaged spectra are denoted as $\langle V_i V_j^* \rangle$.
- 3) The radial current velocity corresponding to a given signal frequency is calculated. The velocity is proportional to the frequency difference from the ideal Bragg frequency, which is computed using the dispersion relation for deep-water gravity waves with wavelength equal to one-half the radar wavelength.
- 4) Boundaries on the radar spectrum delimiting the region due to first-order scatter from the sea are defined. Empirical methods are used to separate the first-order spectrum surrounding the ideal Bragg frequencies from the neighboring lower amplitude, second-order structure, and noise. Note

Manuscript received November 15, 2004; accepted January 19, 2006. The Block Island Sound SeaSonde data were obtained as part of the National Oceanographic Partnership Program funded Front Resolving Observational Network with Telemetry Project. **Associate Editor: L. R. Wyatt.**

B. Lipa is with Codar Ocean Sensors, Portola Valley, CA 94028 USA (e-mail: blipa@codaros.com).

B. Nyden is with Codar Ocean Sensors, Mountain View, CA 94043 USA (e-mail: bruce@codaros.com).

D. S. Ullman is with the Graduate School of Oceanography, University of Rhode Island, Narragansett, RI 02882-1197 USA (e-mail: d.ullman@gso.uri.edu).

E. Terrill is with Scripps Institute of Oceanography, University of California at San Diego, La Jolla, CA 92037 USA (e-mail: eterrill@ucsd.edu).

Digital Object Identifier 10.1109/JOE.2006.886104

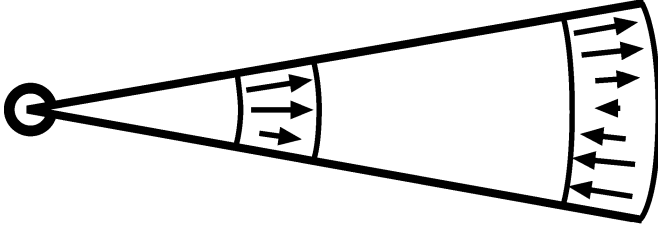


Fig. 1. Schematic illustration showing the increase in radial velocity uncertainty with range. Radar location is indicated by the circle. Shown schematically are two radar range cells (in reality, typically 5° in angular extent). Radial current vectors falling in the radar cells are averaged; their standard deviation increases with range, as more vectors are included in the larger radar cells.

that if the first-order region is set too wide, the anomalous region included at the outer edges will lead to large, incorrect radial velocity vectors.

- 5) Empirical methods are used to judge if a first-order spectral region is contaminated by radar interference, in which case it is excluded from further analysis.
- 6) The voltage cross spectra are then analyzed using the MUSIC algorithm [2], [3] to obtain the direction of arrival of the signal, using either ideal or measured antenna patterns. If ideal patterns are used, they are first corrected for phase and amplitude mismatches between the loop antennas and the monopole. Further detail on MUSIC is given below in Section II-B. This calculation results in the directions of arrival of the signal for each value of the radial velocity and for all range cells.
- 7) The analysis described in step 6) typically produces several velocity values in a given radar cell, which is a segment of a range cell defined by the azimuth angle from the radar and azimuth increment, illustrated schematically in Fig. 1. These values are averaged to give the final output value for that location and the standard deviation is calculated.
- 8) The results are then time-averaged over seven consecutive radial maps. In this paper, we will consider only radial velocities, resulting from the preceding steps 1)–7), i.e., no time averaging.

B. SeaSonde Direction-Finding With MUSIC

The MUSIC algorithm was first presented by Schmidt [2] in 1986. Barrick and Lipa [3] described its application to SeaSonde data. Here, we give a summary of the algorithm as it is implemented in SeaSonde software.

- 1) Voltages V_1 , V_2 , and V_3 from the antennas are modeled as the product of the complex antenna-pattern values and the complex echo signal amplitudes. The signal at a given Doppler shift (and hence a given radial velocity) is assumed to come from at most two directions. This limit is imposed by the information available from the three antennas.

Assuming that the radar echo from the sea comes from a single direction φ_1 , we write the complex zero-mean voltages as a 3×1 matrix formed as the product of the antenna-pattern matrix $[a]$ at that bearing and the signal amplitude s_1

$$\begin{bmatrix} V_1 \\ V_2 \\ V_3 \end{bmatrix} = [a] s_1 \quad \text{where} \quad [a] = \begin{bmatrix} a_1(\varphi_1) \\ a_2(\varphi_1) \\ a_3(\varphi_1) \end{bmatrix}. \quad (1)$$

Assuming that the sea echo comes from two directions φ_1 and φ_2 , the corresponding equation is given by

$$\begin{bmatrix} V_1 \\ V_2 \\ V_3 \end{bmatrix} = [a] \begin{bmatrix} s_1 \\ s_2 \end{bmatrix} \quad \text{where} \quad [a] = \begin{bmatrix} a_1(\varphi_1) & a_1(\varphi_2) \\ a_2(\varphi_1) & a_2(\varphi_2) \\ a_3(\varphi_1) & a_3(\varphi_2) \end{bmatrix} \quad (2)$$

where s_1 and s_2 are the signal amplitudes from the two directions.

- 2) At a given Doppler frequency, we form the covariance matrix C of the complex signal voltages from the three antennas, a 3×3 complex Hermitian matrix

$$C = \begin{bmatrix} V_1 V_1^* & V_1 V_2^* & V_1 V_3^* \\ V_2 V_1^* & V_2 V_2^* & V_2 V_3^* \\ V_3 V_1^* & V_3 V_2^* & V_3 V_3^* \end{bmatrix}. \quad (3)$$

Taking the time average in (3) and substituting (1) or (2) gives

$$\langle C \rangle = \begin{bmatrix} \langle V_1 V_1^* \rangle & \langle V_1 V_2^* \rangle & \langle V_1 V_3^* \rangle \\ \langle V_2 V_1^* \rangle & \langle V_2 V_2^* \rangle & \langle V_2 V_3^* \rangle \\ \langle V_3 V_1^* \rangle & \langle V_3 V_2^* \rangle & \langle V_3 V_3^* \rangle \end{bmatrix} = [a] [S] [a^*]^T \quad (4)$$

where T denotes the transpose, the elements of $\langle C \rangle$ represent the SeaSonde voltage cross spectra, and S is given for a signal from a single direction by

$$S = \langle s_1 s_1^* \rangle \quad (5)$$

and for a signal from two directions by

$$S = \begin{bmatrix} \langle s_1 s_1^* \rangle & \langle s_1 s_2^* \rangle \\ \langle s_2 s_1^* \rangle & \langle s_2 s_2^* \rangle \end{bmatrix}. \quad (6)$$

Ideally, $s_1 s_2^*$ and $s_2 s_1^*$ in (6) average to zero because sea-echo signals are uncorrelated for angular separations as small as 0.5° , as shown by Barrick and Snyder [4]. This is less than the angular spacing of the radar cells.

- 3) An eigenfunction analysis is performed on the covariance matrix. The largest eigenvalues and their corresponding eigenvectors represent the sea echo, whereas the smaller eigenvalues represent noise. When the signal is from two/one directions, ideally there are two/one nonzero eigenvalues. In practice, the noise eigenvalues are finite but small compared with the signal eigenvalues.
- 4) The direction(s) of arrival of the signal(s) are determined using the fundamental principle behind MUSIC: The signal eigenvector at the correct bearing is orthogonal to all the noise eigenvectors. The algorithm finds the angle(s) at which this occurs. This procedure is carried out first assuming that the signals are coming from two directions, to give the two angles and the 2×2 signal matrix termed “dual-angle solutions.” Then, it is assumed that the signal comes from only one direction. The calculation gives the single optimum angle and the corresponding signal power termed a “single-angle” solution.
- 5) The dual-angle solution is then tested to judge its validity. Three criteria are defined based on the following observations. 1) If the echo signal is indeed coming from two directions, the two signal eigenvalues and the corresponding values of signal power will be much greater than the noise values. 2) The two signal eigenvalues and powers should

be reasonably close in magnitude, as if one signal power or eigenvalue is far less than the other; it follows that most energy comes from a single direction which would cast doubt on the dual-angle solution. 3) As discussed previously, the off-diagonal elements of the signal matrix S are ideally zero and in practice should be much smaller than the diagonal elements for a valid dual-angle solution.

Defining three parameters P_1 , P_2 , and P_3 (termed the MUSIC parameter set), these observations lead to the following three criteria for a valid dual-angle solution.

- The ratio of the largest covariance matrix eigenvalue to the second largest must be less than P_1 .
- The ratio of the largest of two signal powers $\langle s_1 s_1^* \rangle$ and $\langle s_2 s_2^* \rangle$ to the smallest must be less than P_2 .
- For the signal matrix S defined by (6), the ratio of the product of the diagonal elements to the product of the off-diagonal elements must be greater than P_3 .

If any of these tests are failed by the dual-angle solution, it is rejected and the single angle solution is accepted.

To illustrate when single/dual angle solutions apply, we note that for the case of a uniform current flowing parallel to a straight shore, single-angle solutions will be produced at every azimuth around a range cell, as the radial component of the velocity is then a single-valued function of azimuth. In the unlikely situation that a uniform current flows perpendicular to a straight coast, all the solutions would be dual angle except for the azimuth normal to the coastline, as the radial velocity components occur in pairs around the range cell. Ideally, the parameter set would produce a percentage of dual angle solutions which is consistent with that calculated from the derived radial current map. With the software presently in use, it is necessary to preset the MUSIC parameters to fixed values, although obviously a single parameter set may not be appropriate for all current velocity patterns as the percentage of dual-angle solutions varies with time and location.

To demonstrate the proportion of dual-angle solutions in a typical measurement, the percentage of dual-angle solutions obtained for three different MUSIC parameter sets are plotted in Fig. 2 for a data set consisting of seven days of 10-min radar spectra measured by the SeaSonde located at Misquamicut, RI. The entire first-order region (for both positive and negative Doppler frequencies) and for all range cells were analyzed to give radial velocities. Results for the dual-angle percentages are plotted in black, dark gray, and light gray for the MUSIC parameter sets [30, 15, 1.8], [20, 10, 3], and [10, 5, 8]. For the standard SeaSonde parameter set [20, 10, 3] in use until recently, there are typically less than 20% dual-angle solutions. This parameter set was chosen by simulating typical current scenarios and minimizing the differences between the input currents and the calculated values. It has recently been replaced with the set [40, 20, 2], which yields more dual-angle solutions and fewer gaps in the radial map.

C. Use of Measured Antenna Patterns

SeaSonde radial velocities are calculated using antenna patterns that are either ideal or measured. To measure the patterns, a transponder is placed on a boat which traverses an arc at constant range transmitting signals that are picked up by the Sea-

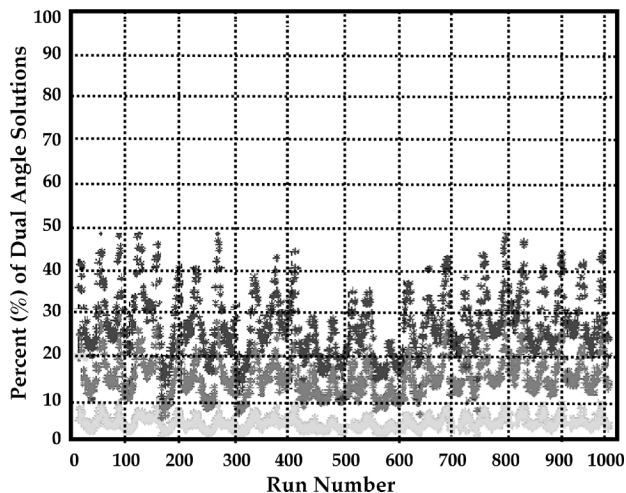


Fig. 2. Percentage of Doppler points that yield a dual-angle solution versus run number using different MUSIC parameter sets $[P_1, P_2, P_3]$: black [30, 15, 1.8], dark gray [20, 10, 3], and light gray [10, 5, 8] plotted versus the run number. Each run consists of analysis of 10-min-averaged spectra from Misquamicut measured from August 26, 2000 to September 2, 2000. Ideal antenna patterns were used in analysis.

Sonde receiver. The received signals are then analyzed to produce the complex antenna voltage patterns to be used in the signal analysis.

1) *Effects of Smoothing the Antenna Patterns:* When measured antenna patterns are used in the analysis of SeaSonde voltage cross spectra, they are often found to contain too much structure for the software to handle, given the amount of information available from three antennas. Persistent gaps result in the radial velocity maps at specific azimuth angles, often associated with local pattern amplitude maxima, with radial velocities crowding onto the gap boundaries. To ameliorate this problem, antenna patterns are smoothed over 10° – 20° using a running mean over angle. To illustrate the effects of antenna-pattern smoothing, radial patterns resulting from both smoothed and unsmoothed patterns are shown in Fig. 3. It can be seen that with the smoothed patterns, gaps in the coverage are reduced. Using ideal patterns, radial current patterns are usually uniformly filled in, but tests show that the radial velocities produced with ideal antenna patterns are usually less accurate; see, for example, [5].

2) *Effects of Restricted Antenna Patterns:* In some situations, the boat transporting the transponder cannot go all the way up to the shore because of obstacles, kelp beds, shallow water, etc. The resulting antenna-pattern measurements then have gaps at the coast and the full angular range of the sea echo is not covered by the pattern measurement. This results in radial vectors crowding onto the radial spoke on the antenna-pattern boundary.

To illustrate the effects of antenna-pattern truncation, we studied radial velocities measured by a SeaSonde at Point Loma, CA (see Fig. 4 for the configuration). As the radar site is situated at the tip of a peninsula, water coverage is almost 360° for ranges less than about 10 km, where the antenna pattern was measured. However, due to the presence of floating kelp beds, the boat carrying the transponder was unable to approach the northern coast and as a result the antenna pattern is cut off to the northwest. Fig. 4(a) shows a radial velocity map obtained

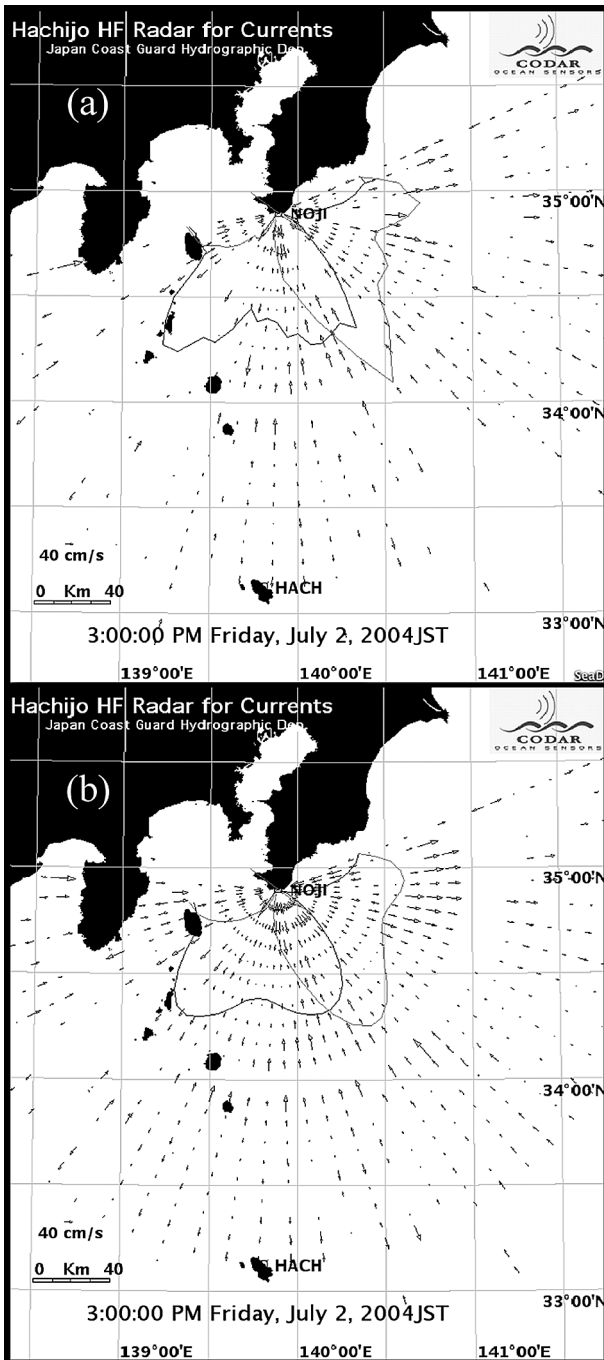


Fig. 3. Radial patterns for Nojima, Japan, obtained with (a) unsmoothed measured antenna patterns and (b) measured antenna patterns smoothed over 20° . Antenna-pattern amplitude ratios are shown, i.e., the ratios of loop antenna amplitudes to the monopole amplitude. Note that gaps in the coverage are reduced in (b). Range cell 10 is empty due to radar interference in the corresponding radar spectrum.

using the measured pattern: The radial velocities can be seen to crowd onto the northwest antenna-pattern boundary. There is reduced water coverage for the outer range cells. Ideally, the antenna pattern for each range cell should be adjusted to cover only the open water for that range cell; however, in this paper, we used the same antenna pattern for all range cells. This results in vectors falling over the land for some outer range cells.

To investigate the effects on radial current patterns of such truncation of the antenna pattern, we artificially further truncated the Point Loma antenna pattern. As antenna-pattern points were removed from the northwest edge of the pattern, the crowded spokes in the radial map moved to the new pattern boundary [see Fig. 4(b)]. A similar effect resulted when antenna-pattern points were removed from the northeast edge of the pattern [see Fig. 4(c)]. It appears that the radial velocities on the crowded edge spokes contain solutions from signals coming from directions not covered by the antenna pattern.

It is significant to note that the radial vectors away from the pattern boundaries do not appear to be affected by the additional truncation of the antenna pattern. Therefore, to deal with truncated antenna patterns, it seems reasonable to eliminate radial velocities occurring on the boundary angles of the pattern and accept the remainder of the map as valid. SeaSonde software now uses this procedure.

III. RADIAL VELOCITY QUALITY CHECKS

In this section, we describe internal consistency checks that can be used to assess the quality of radial velocity maps.

A. Visual Inspection

Maps of radial current velocities provide much information on system performance. Even a casual glance at a radial map can be very revealing. Here are some examples:

- 1) When measured patterns are used, consistent gaps in the angular coverage at certain azimuth angles over extended periods indicate that the software may have difficulties with sharp variations in the pattern and smoothing of the antenna pattern may be required.
- 2) If ideal antenna patterns are used, a large number of radial vectors falling over land behind the radar is probably due to inaccuracies in the input parameters used in the analysis, e.g., phase correction factors and MUSIC parameters.
- 3) The presence of large anomalous vectors indicates that the first-order region is being set too wide, resulting in the inclusion of higher order structure.
- 4) Comparing the radial vectors output by two radars at points along a baseline between the sites provides a simple test of system performance: The radial vectors produced by the two radars at the same location should be consistent within their error bars, which include the effects of radar cell size differences discussed later.

Fig. 5 shows examples of radial velocity maps produced by SeaSondes at Hachijo and Nojima, Japan. These maps, which were obtained using ideal antenna patterns, are well filled out and only a small fraction of the radial vectors fall over land. However, the radial velocities from the two sites along the baseline between them are not consistent, particularly close to Nojima. We describe the probable cause of this inconsistency in Section V. There is a missing range cell in the Nojima map; radial vectors from this range cell have been eliminated due to spectral contamination caused by radar interference.

B. Uncertainties in Radial Velocities

1) *Sources of Uncertainty:* Assuming that the radar is operating correctly, we can identify the following sources of un-

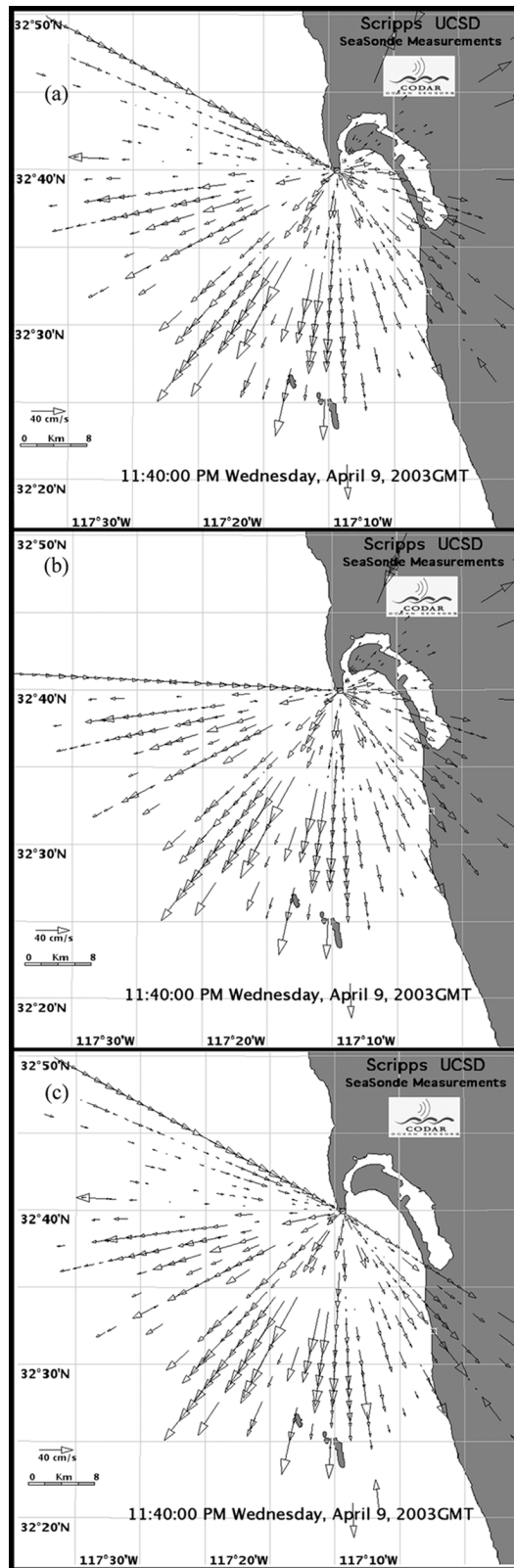


Fig. 4. (a) Example of the effect on the radial velocities of truncated measured antenna patterns at Point Loma, at 23:40:00Z, on April 9, 2003. Antenna patterns do not go up to the northern coastline. This results in radial velocities crowding on the edge-spoke at the antenna-pattern boundary. (b) Example of the effect of truncated measured antenna patterns at Point Loma, at 23:40:00Z, on April 9, 2003. Antenna patterns artificially truncated by a further 25° on the northwest edge. The crowded spoke is now at new antenna-pattern boundary. The remainder of the radial velocity map is unchanged. (c) Example of the effect of truncated measured antenna patterns at Point Loma, at 23:40:00Z, on April 9, 2003. Antenna pattern artificially truncated by 100° on the northeast edge. There are now crowded spokes at both antenna-pattern boundaries. The remainder of the radial map is virtually unchanged.

certainty in the radial velocities: variations of the radial current component within the radar scattering patch, variations of the

current velocity field over the duration of the radar measurement, statistical noise in the radar spectral data, errors/simplifi-

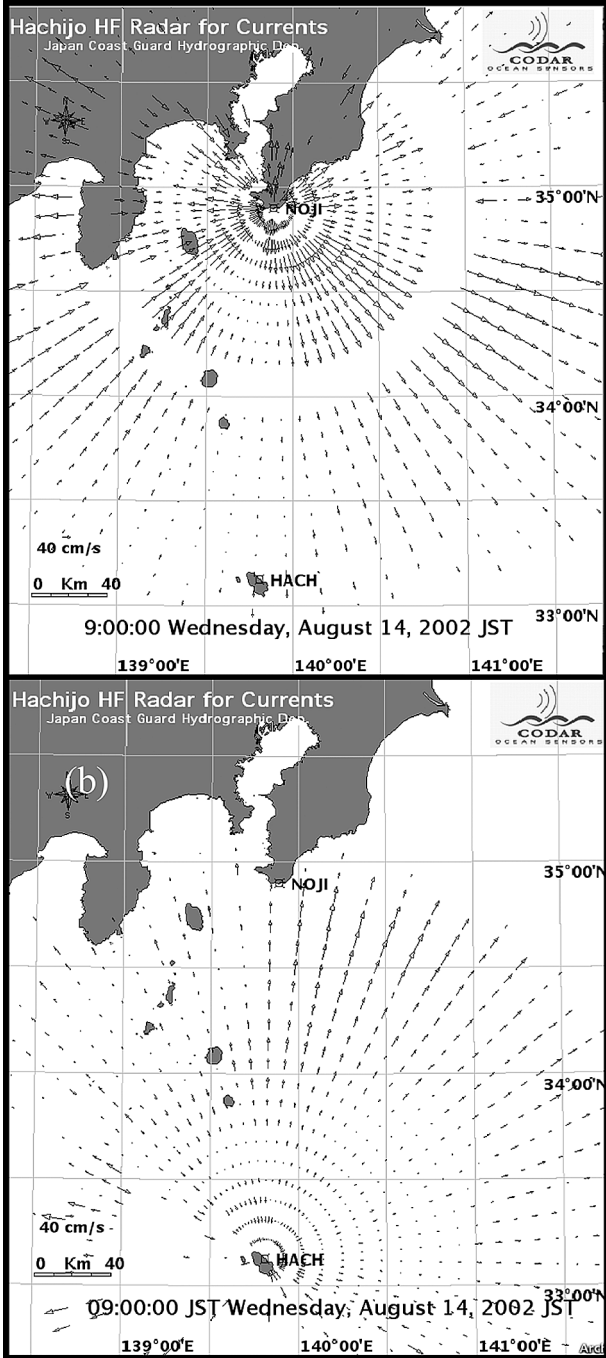


Fig. 5. Example of radial current velocity vectors measured by SeaSondes on Tokyo Bay, Japan, at 09:00:00JST, on August 14, 2002. (a) Nojima. (b) Hachijo. Note the inconsistency of the radial velocities measured by the two systems close to Nojima.

cations in the analysis, for example the use of incorrect antenna patterns and analysis parameters, and errors in the empirical determination of first-order region boundaries.

2) *Estimation of Uncertainties in Unmerged Radial Velocities*: From the analysis of a 10-min voltage spectral average, we collect all the radial vectors falling on a given radar cell (see Fig. 1 for a schematic diagram). The mean and standard deviation of these vectors represent the SeaSonde radial current and its uncertainty at that location. Standard deviations estimated in

this simple way represent a lower bound on the actual uncertainty in the current velocity. For example, errors due to contaminated radar spectra or incorrect first-order region boundaries will not be included in the estimate. Even when this uncertainty is high, the average often does not vary significantly with time. Thus, SeaSonde measurements appear stable as a function of time and two SeaSondes operated side-by-side will produce similar results. It can be a different matter when a SeaSonde area measurement is compared with a buoy point measurement. Differences in the two velocity measurements do not necessarily indicate inconsistency, if they are less than the error bars.

3) *Baseline Tests of Data Quality*: Baseline tests are consistency checks on radial velocities from two SeaSondes at points on the baseline joining the two sites. Ideally, the two systems will give the same estimates of radial velocity, differing only in the sign. However, at points on the baseline away from the midpoint, radial velocities from the two radars represent averages over radar cells of different sizes, and will differ in the presence of horizontal velocity shear. For consistency, such velocity deviations should be accounted for by the calculated uncertainties. Paduan *et al.* [5] describe baseline tests performed for the Monterey Bay SeaSonde network, looking at data at the midpoint of the baseline. We here develop methods that apply to the entire baseline.

Taking a baseline between two SeaSondes at sites α and β , we define the following parameters: x is the distance from site α along the baseline and $v_\alpha(x)$ and $v_\beta(x)$ are the radial velocities measured by the two SeaSondes with standard deviations $\sigma_\alpha(x)$ and $\sigma_\beta(x)$. The root-mean-square (rms) velocity $A(x)$, rms baseline deviation $B(x)$, and rms standard deviation $S(x)$ are defined as follows:

$$A(x) = \sqrt{\left\langle \frac{v_\alpha^2(x) + v_\beta^2(x)}{2} \right\rangle} \quad (7)$$

$$B(x) = \sqrt{\left\langle \frac{(v_\alpha(x) + v_\beta(x))^2}{2} \right\rangle} \quad (8)$$

$$S(x) = \sqrt{\left\langle \frac{\sigma_\alpha^2(x) + \sigma_\beta^2(x)}{2} \right\rangle}. \quad (9)$$

In (7)–(9), the angular brackets again represent averages over time. At least a thousand consecutive estimates are used to produce the time average. Using the sign convention that radial velocities pointing toward/away from the radar are positive/negative, for no data imperfections at a given point on the baseline, the radial velocities $v_\alpha(x)$ and $v_\beta(x)$ are equal and opposite, and their sum is zero, as is $B(x)$ as defined by (8). In practice, $B(x)$ is nonzero due to imperfections in the spectral data and its analysis.

From (7) and (8)

$$\begin{aligned} B^2 &= A^2 + \langle v_\alpha(x)v_\beta(x) \rangle \\ &\approx A^2 - \left\langle (v_\alpha(x))^2 \right\rangle \end{aligned} \quad (10)$$

as $v_\alpha(x) \approx -v_\beta(x)$ along the baseline.

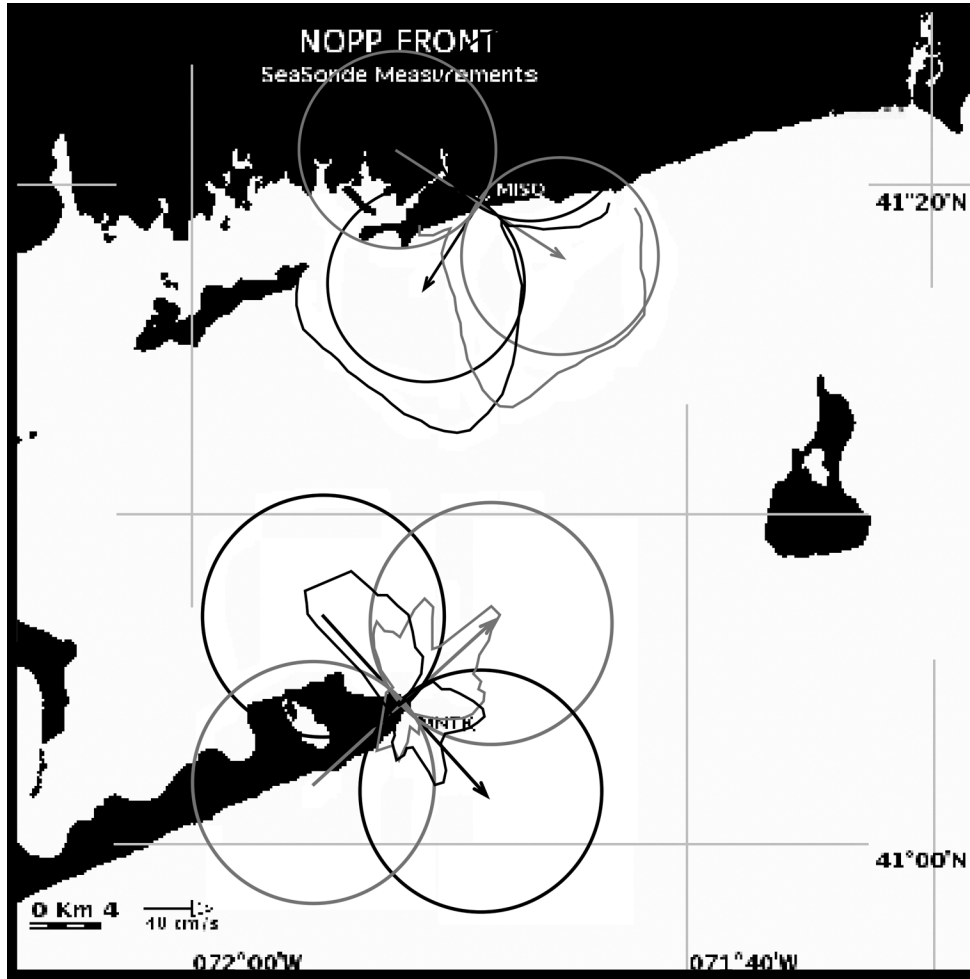


Fig. 6. Standard-range SeaSondes at Misquamicut (MISQ) and Montauk (MNTK) near Block Island Sound. Ideal and measured antenna-pattern amplitude ratios are shown.

Expressing the radial velocities within a radar cell relative to their true values at position x on the baseline

$$v_{\alpha}(x) = v_{\alpha}^{\text{True}}(x) + \Delta v_{\alpha}(x); v_{\beta}(x) = v_{\beta}^{\text{True}}(x) + \Delta v_{\beta}(x) \quad (11)$$

where $\Delta v_{\alpha}(x)$ and $\Delta v_{\beta}(x)$ contain all the velocity differences from the true baseline value due to horizontal velocity shear in the radar cell and other sources of uncertainty outlined in Section III-B

$$v_{\alpha}^{\text{True}}(x) + v_{\beta}^{\text{True}}(x) = 0. \quad (12)$$

Substituting (11) and (12) into (8) gives

$$B(x) = \sqrt{\left\langle \frac{\left(v_{\alpha}^{\text{True}}(x) + \Delta v_{\alpha}(x) + v_{\beta}^{\text{True}}(x) + \Delta v_{\beta}(x) \right)^2}{2} \right\rangle} \\ = \sqrt{\left\langle \frac{(\Delta v_{\alpha}(x) + \Delta v_{\beta}(x))^2}{2} \right\rangle}. \quad (13)$$

Ignoring correlations between $\Delta v_{\alpha}(x)$ and $\Delta v_{\beta}(x)$, it follows from (13) that rms baseline deviation $B(x)$ should

equal the rms standard deviation $S(x)$, as by definition $\sigma_{\alpha}(x) = \sqrt{\langle \Delta v_{\alpha}^2(x) \rangle}$ and $\sigma_{\beta}(x) = \sqrt{\langle \Delta v_{\beta}^2(x) \rangle}$. Equations (10) and (13) then define the following approximate tests for the data, using measured antenna patterns:

Test 1: $B^{\text{meas}}(x) < A^{\text{meas}}(x)$ for nonzero radial velocities on the baseline (14)

Test 2: $B^{\text{meas}}(x) \approx S^{\text{meas}}(x)$. (15)

A third test compares baseline deviations for ideal and measured antenna patterns intended for use when the measured patterns are significantly distorted from the ideal values. For an accurate antenna-pattern measurement, velocity estimates made with measured patterns should be more accurate than those made assuming ideal patterns which poorly approximate physical reality. Hence, one would expect baseline deviations obtained using measured pattern to be less than those for ideal patterns

Test 3: $B^{\text{meas}}(x) < B^{\text{ideal}}(x)$. (16)

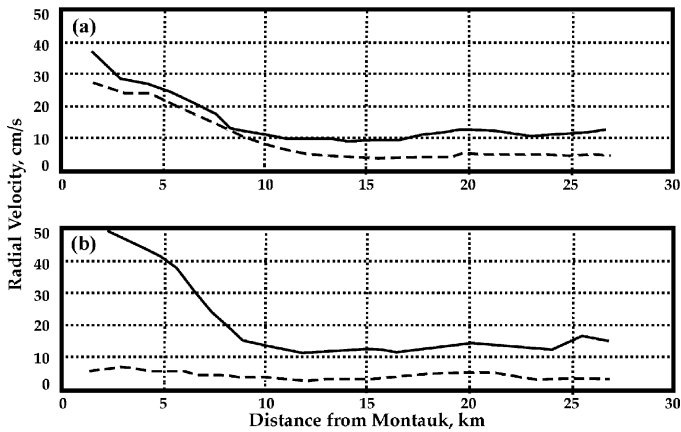


Fig. 7. rms radial velocities and their uncertainties for Misquamicut (upper) and Montauk (lower) obtained by averaging over SeaSonde hourly results obtained along the baseline between the sites during November 11–17, 2000. Solid line: rms radial velocity. Dashed line: averaged uncertainty.

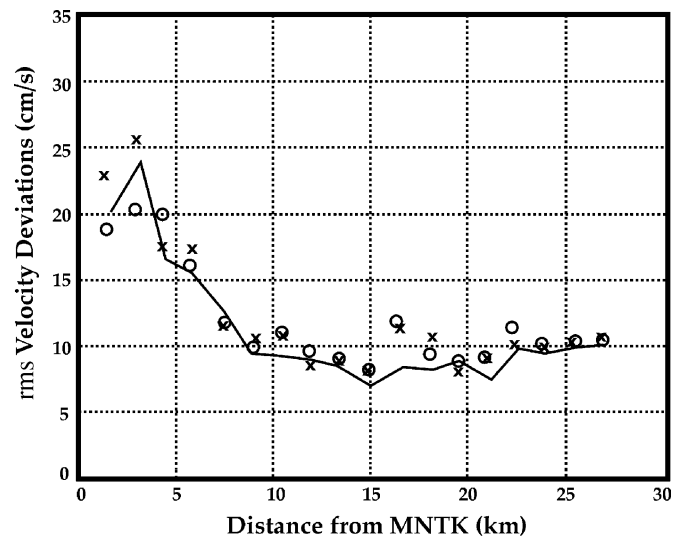


Fig. 8. rms baseline deviations (centimeter per second) versus distance from Montauk (kilometers) for different averaging times. Circles: 3 h. Continuous line: 1 h. Crosses: 10 min. Spectra measured November 11–17, 2000. Measured antenna patterns used in analysis.

IV. EXAMPLES OF BASELINE ANALYSIS

In this section, we illustrate baseline data analysis for two baselines with contrasting results. For the baseline between two standard-range SeaSondes over Block Island Sound, the tests were passed successfully and interpretation of the results proved quite revealing of the nature of SeaSonde current measurements. For the baseline between two long-range SeaSondes over Tokyo Bay, the first results were less encouraging. Further study showed that the large deviations arose from use of noisy radar spectra. Acceptable results were obtained by placing a lower limit on the signal-to-noise ratio.

A. Block Island Sound

This section describes analysis of radial velocities measured at points along the Block Island Sound baseline between Misquamicut and Montauk. See Fig. 6 for the site locations and relative antenna-pattern amplitudes, which for Misquamicut closely

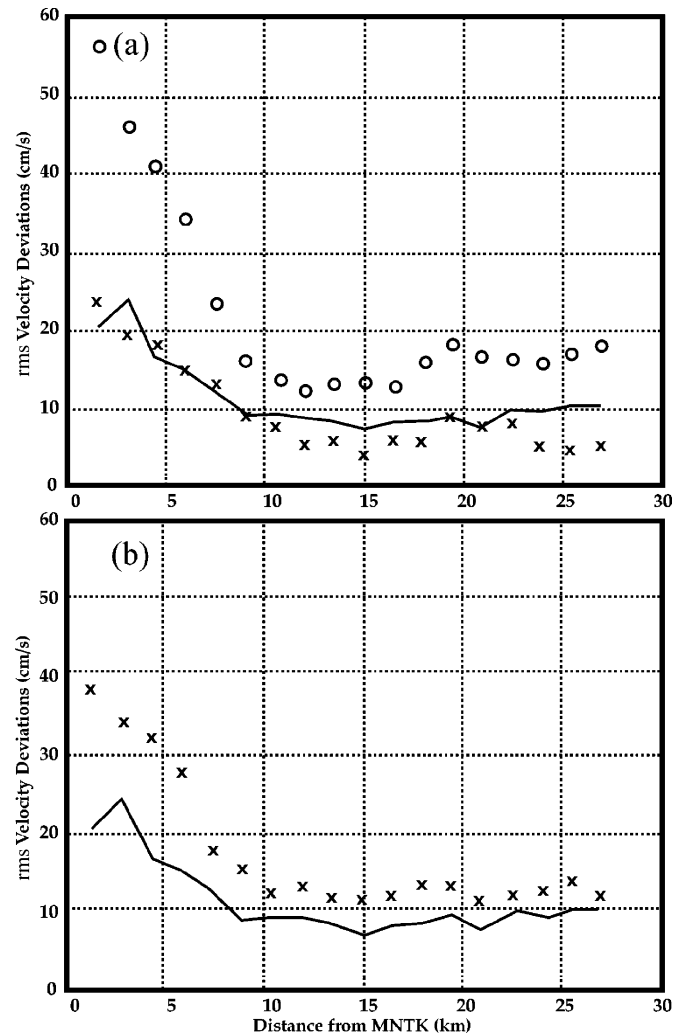


Fig. 9. (a) Baseline test parameters versus distance (km) along the baseline from Montauk, obtained by averaging over SeaSonde 10-min-averaged spectra November 11–17, 2000. Solid line: rms baseline deviations (cm/s); Crosses: rms sum of the spatial uncertainties (cm/s). Circles: rms velocity (cm/s). (b) rms baseline deviations (cm/s), versus distance (km) along the baseline from Montauk, obtained by averaging over SeaSonde 10-min-averaged spectra November 11–17, 2000. Solid line: measured antenna patterns. Crosses: ideal patterns used in analysis.

approximate ideal values. The systems operated at transmit frequencies of approximately 25 MHz and the range-cell width was 1.5 km. Independent estimates of the radial velocity were made from averaged spectra measured November 11–17, 2000. The baseline lies over about 27 km of open ocean. The current velocity and horizontal velocity shear increase close to Montauk, as the current swirls around the Montauk point. The systems were performing optimally at this time; the antenna patterns were checked and considered sound; and first-order region settings were examined and found to be accurate. Remaining sources of uncertainty were, therefore, statistical noise in the data, variations of oceanographic conditions during the 10-min spectral averaging period, and horizontal shear within the radar cell.

1) *Averaged Results for the Individual Sites:* In Fig. 7, we plot the rms radial velocity together with the rms standard deviation for the two sites at points along the baseline. Values are

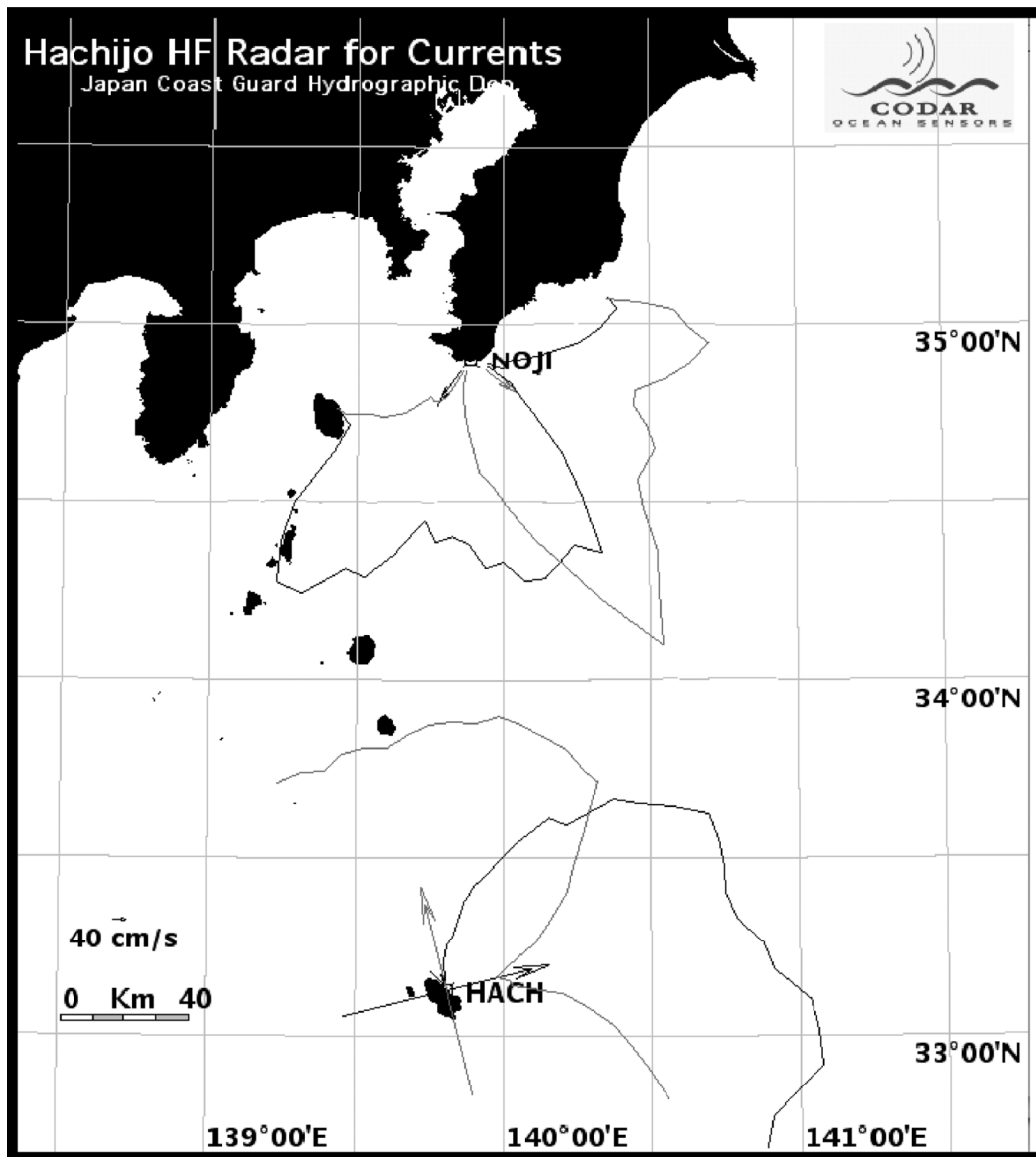


Fig. 10. Long-range SeaSondes at Hachijo and Nojima, Japan. Unsmoothed, measured antenna-pattern amplitudes are shown.

obtained by averaging baseline radial velocities over the whole period. Ideally, the rms speeds from the two sites would be identical. Clearly, however, close to Montauk at a given location on the baseline, the speed measured from Montauk is much larger than that measured from Misquamicut, and the Misquamicut rms standard deviation becomes almost as large as the speed itself. This can be explained as follows: a) There is a large horizontal velocity shear close to Montauk and b) the Misquamicut radar cell size is large as it is distant from the radar. Therefore, when the velocities from the radar cell are averaged, there is a lot of averaging-down due to the large horizontal shear within the cell, yielding a value much lower than the extreme value. In contrast, at this location, the Montauk radar cell size is small, as it is close to the radar, and there is much less averaging-down, leading to a higher velocity value and a lower spatial uncertainty. This effect is illustrated schematically in Fig. 1.

2) *Averaging Times*: If the major source of uncertainty is statistical noise, uncertainties in radial velocities would be in-

versely proportional to the square root of the averaging time used for the radar cross spectra. However, for lengthy averaging times, the current field may undergo a significant change over the time period, resulting in increased uncertainties.

In a study aimed at optimizing the spectral averaging time, baseline deviations were calculated for three averaging periods: 10 min, 1 h, and 3 h. The results are shown in Fig. 8. It can be seen that the baseline deviations differ by less than 25% between the three spectral averaging times, indicating that the uncertainties are not statistical in nature but must arise mainly from bias. One-hour spectral averaging is shown to be optimal, as it produces slightly lower baseline deviations around the midpoint where the radar cells for the two sites have equal size.

The similarity between the baseline results for the three spectral averaging times indicates that in this case the current field did not change appreciably over these time scales. At the midpoint, the rms baseline deviation is about 8 cm/s, which represents the intrinsic accuracy of the velocity measurement. Close

to Montauk, the large baseline deviations are probably due to horizontal current shear within the radar cell.

3) *Baseline Tests*: Parameters for the three baseline tests defined by (7)–(9) are plotted in Fig. 9 versus distance along the baseline from one of the sites.

Test 1) Fig. 9(a) shows that the rms baseline deviations are less than the rms velocities for all values of x , consistent with (14).

Test 2) Fig. 9(a) shows that the rms baseline deviations $B(x)$ are approximately equal to the rms standard deviations $S(x)$, consistent with (15). Therefore the large baseline deviations close to Misquamicut are accounted for by the large uncertainties.

Test 3) It can be seen from Fig. 9(b) that the baseline deviations are always lower for measured patterns than for ideal patterns, consistent with (16) and supporting an accurate antenna-pattern measurement. Thus, the three baseline tests are passed successfully in this case.

B. Tokyo Bay

As another example, we consider the baseline between SeaSondes at Nojima and Hachijo near Tokyo Bay. See Fig. 10 for site locations and relative smoothed antenna-pattern amplitudes. The long-range SeaSonde sites operated at approximately 5-MHz transmit frequency and the range-cell width was about 10 km. Estimates of the radial velocity were made every 30 min from September 15, 2003 to October 15, 2003. The baseline lies over about 180 km of open ocean.

Parameters for the three baseline tests are plotted in Fig. 11 versus distance along the baseline from Hachijo.

Test 1) Fig. 11(a) shows that rms baseline deviations $B(x)$ (plotted as a continuous line) are less than the rms velocities $A(x)$ (plotted as circles), over most of the baseline; however, they converge close to Hachijo.

Test 2) Fig. 11(a) shows that away from the midpoint of the baseline, rms baseline deviations considerably exceed the rms standard deviations (plotted as crosses), violating (15) in this region.

Test 3) It can be seen from Fig. 11(b) that the baseline deviations for measured and ideal patterns are not significantly different, in spite of the fact that the antenna patterns are significantly distorted (see Fig. 10).

Results from the baseline tests indicate problems either with the radar spectra or with the analysis. Quite often, substantial angular sectors neighboring the baseline near Nojima have opposing radial velocities (for example, see Fig. 5). These discrepancies appear to be due to low signal-to-noise ratios. When significant portions of the first-order region are below the noise, which occurs more frequently at distant ranges, the derived radial velocities are unreliable (see Section V).

V. ANOMALOUS CURRENT VECTORS FROM NOISY SPECTRA

When much of the Bragg region is near or under the noise level, the portion above the noise will have a restricted frequency range. The range in radial current speed will, therefore, be less than that existing on the ocean surface. There is no direct way to tell from the data whether larger radial speeds corresponding

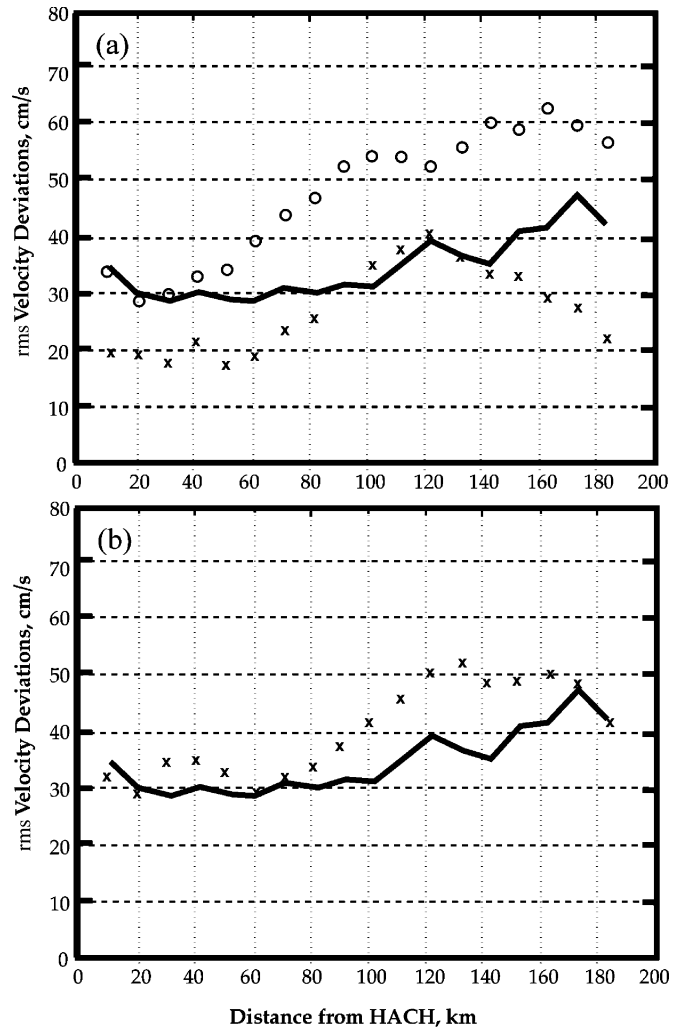


Fig. 11. (a) Baseline test parameters versus distance (km) along the baseline from Hachijo, 30-min-averaged spectra September 15–October 15, 2003. Solid line: rms baseline deviations (cm/s). Crosses: rms sum of the spatial uncertainties (cm/s). Circles: rms velocity (cm/s). (b) rms baseline deviations (cm/s) versus distance (km) along the baseline from Hachijo, 30-min-averaged spectra September 15–October 15, 2003. Solid line: measured antenna patterns. Crosses: ideal patterns used in analysis.

to spectral values outside the first-order boundaries are not produced because 1) there are no such radial speeds or 2) the corresponding radar spectra are below the noise level.

Each radar cell (contained within neighboring range rings and azimuth boundaries, as illustrated schematically in Fig. 1) contains different current velocities due to horizontal velocity shear on the ocean surface. A typical solution produces several velocity values at a given location, presumably due to the presence of different current velocities within the radar cell. These values are averaged to give the final output value for that location. However, for noisy radar spectra, the range in velocity values produced by the analysis is limited. Thus, when the average is taken, the result will be biased.

Analysis of noisy SeaSonde spectra leads to radial velocities that do not adequately represent the current velocity field. This is believed to be the cause of the failure of the baseline tests for Tokyo Bay. We reran the baseline tests eliminating cross spectra for which the signal-to-noise ratios are below 25 dB (all

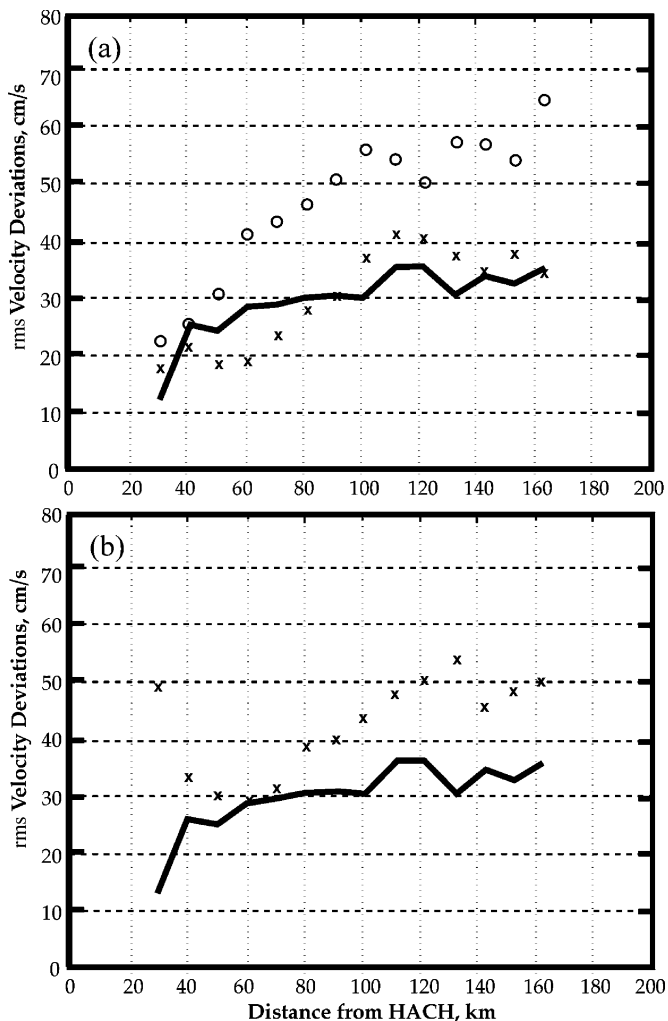


Fig. 12. Data as in Fig. 11, but analysis is restricted to radar cross spectra for which the signal-to-noise ratio exceeds 25 dB for all three antennas.

antennas). Results are shown in Fig. 12. Applying the baseline tests gives the following.

- Test 1) Fig. 12(a) shows that the rms baseline deviations are less than the rms velocities over the whole baseline.
- Test 2) Fig. 12(a) shows that the rms baseline deviations $B(x)$ are approximately equal to the rms standard deviations $S(x)$.
- Test 3) It can be seen from Fig. 12(b) that the baseline deviations are always lower for measured patterns than for ideal patterns, supporting an accurate antenna-pattern measurement. Therefore, the tests are passed successfully when the restriction on signal-to-noise ratio is applied.

In addition to high baseline deviations, analysis of noisy SeaSonde spectra leads to inaccurate total vectors when the resulting radial velocities are combined with those from a second radar site. This is illustrated in Fig. 13(a) for a sample of problem data identified and provided by the University of North Carolina, Chapel Hill. Large current velocity vectors that oppose the Gulf Stream can be seen at the outer edge of the coverage. These anomalous vectors disappeared when we

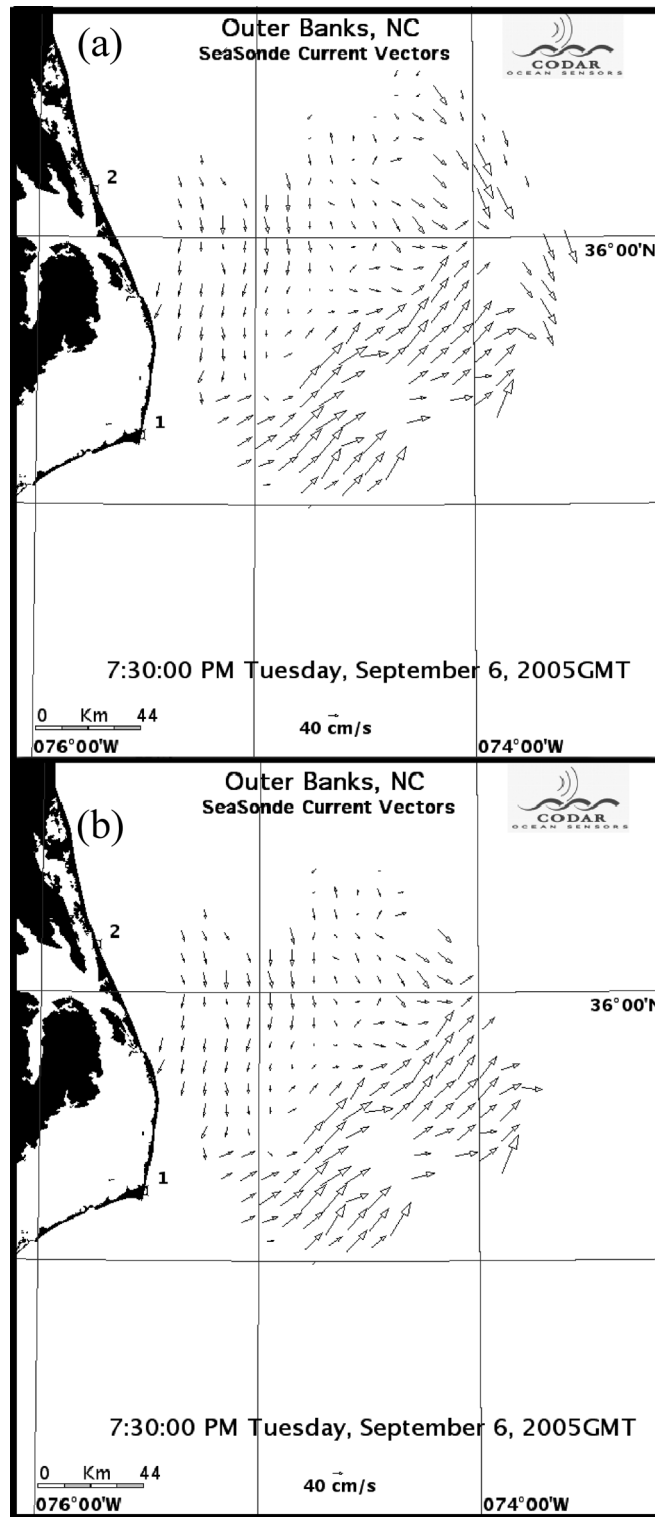


Fig. 13. (a) Total velocity vectors measured by the University of North Carolina SeaSonde network on September 6, 2005. Note anomalous vectors opposing the Gulf Stream at the outer edge of the coverage. (b) Data as in Fig. 13(a), but analysis is restricted to radar cross spectra for which the signal-to-noise ratio exceeds 20 dB for all three antennas. No anomalous vectors.

eliminated cross spectra for which the signal-to-noise ratios are below 20 dB (all antennas) [see Fig. 13(b)].

VI. CONCLUSION

We have described methods used for the derivation of SeaSonde radial velocities from measured sea-echo voltage cross spectra, including the application of the MUSIC direction-finding algorithm and methods for dealing with problems arising when measured antenna patterns are used.

Simple visual checks/diagnostics of radial velocity maps have been outlined. Empty sectors indicate too much structure in measured antenna patterns; vectors over land occurring when ideal antenna patterns are used probably indicate incorrect phase correction factors; and large erratic radial vectors indicate errors in boundaries set for the first-order spectral region used for radial current determination.

We have defined quantitative tests based on the difference in radial velocities measured by two radar systems on the baseline that joins them. These tests are illustrated by application to two radar networks. For the standard-range Block Island network, the tests are passed successfully. Results obtained along the Block Island baseline indicate that baseline deviations are insensitive to spectral averaging times less than 3 h, indicating for this case that the effects of statistical noise and time variations in the current field appear to be relatively low. We hypothesize that uncertainty estimates for unmerged radial vectors represent a measure of horizontal velocity shear within the radar cell. This hypothesis could be experimentally verified by a comparison of SeaSonde radial velocity uncertainties with buoy measurements of horizontal velocity shear within the radar cell.

For the long-range Tokyo Bay network, baseline tests failed when all cross spectra were used in the analysis. This appears to be due to low signal-to-noise ratios far from the radar sites causing much of the first-order region of the spectrum to be eliminated from the analysis. This problem leads to anomalous radial and total velocities in the SeaSonde output.

Radial velocities from noisy spectra should not be included in the output radial velocity files, as they cannot adequately represent the radial current velocity field. We need to develop methods to eliminate noisy cross spectra from the analysis for radial velocities, based on signal-to-noise ratios or other criteria.

ACKNOWLEDGMENT

The authors would like to thank Dr. D. E. Barrick and Dr. A. D. Kirwan for numerous helpful discussions, the Montauk Point Lighthouse Museum, the U.S. Coast Guard, and the Rhode Island Department of Environmental Management for allowing use of their properties for the SeaSonde installations, the Scripps Institution of Oceanography for access to data from their SeaSondes, the Environmental and Oceanographic Research Division of the Hydrographic and Oceanographic Department, Japan Coast Guard, for providing access to the SeaSonde data described in this paper, and the University of North Carolina for access to data from their SeaSondes

REFERENCES

- [1] B. J. Lipa and D. E. Barrick, "Least-squares methods for the extraction of surface currents from CODAR crossed-loop data: Application at AR-SLOE," *IEEE J. Ocean. Eng.*, vol. OE-8, no. 4, pp. 226–253, Oct. 1983.
- [2] R. O. Schmidt, "Multiple emitter location and signal parameter estimation," *IEEE Trans. Antennas Propag.*, vol. AP-34, no. 3, pp. 276–280, Mar. 1986.

- [3] B. J. Lipa and D. E. Barrick, "Comparison of Direction-Finding and Beam-Forming in HF Radar Ocean Surface Current Mapping" National Oceanic and Atmospheric Administration, Rockville, MD, Phase 1 SBIR Final Rep., 1996, Contract No. 50-DKNA-5-00092.
- [4] D. E. Barrick and J. A. Snyder, "The statistics of HF sea-echo Doppler spectra," *IEEE Trans. Antennas Propag.*, vol. AP-25, no. 1, pp. 19–28, Jan. 1977.
- [5] J. D. Paduan, K. C. Kim, M. S. Cook, and F. P. Chavez, "Calibration and validation of high frequency radar ocean surface current observations," *IEEE J. Ocean. Eng.*, vol. 31, no. 4, pp. 862–875, Oct. 2006.



Belinda Lipa received the Ph.D. degree in theoretical physics from the University of Western Australia, Perth, Australia, in 1969.

She was a Research Associate at Stanford University, Stanford, CA, from 1974 to 1978, working on the interpretation of narrow-beam HF radar sea echo to give parameters of the directional ocean wave spectrum, and continued this work at SRI International, Menlo Park, CA. In 1980, she formed a private company with the purpose of developing software to give ocean surface information from sea echo received by

small broadbeam HF radar systems. Since 1986, she has been a Vice President of Codar Ocean Sensors, Portola Valley, CA, a small company that develops and markets the SeaSonde, a compact radar for the measurement of ocean surface current maps and directional wave spectra in coastal waters.



Bruce Nyden received the M.A. degree in geography (remote sensing) from San Diego State University, San Diego, CA, in 2000.

He was a Research Technician at San Diego State University from 1991 to 2000 and worked on change detection of coastal salt marsh vegetation using low-altitude multispectral imagery. In 2000, he began work for Bodega Marine Laboratory, University of California-Davis, Davis, where he was a Geographic Information System and Marine Instrumentation Specialist. In 2002, he joined Codar Ocean Sensors,

Mountain View, CA, where he currently manages the customer support group.



David S. Ullman received the B.E. degree from Stevens Institute of Technology, Hoboken, NJ, in 1981 and the M.S. and Ph.D. degrees in coastal oceanography from Stony Brook University, Stony Brook, NY, in 1984 and 1996, respectively.

Since 1999, he has been an Assistant Marine Research Scientist at the Graduate School of Oceanography, University of Rhode Island, Narragansett. He is an Observational Physical Oceanographer whose research focuses on processes responsible for circulation and mixing in the coastal ocean. He has been

operating a three-site standard-range SeaSonde system covering Block Island Sound and the continental shelf south of Rhode Island for the past six years and has published several papers utilizing these data. Recently, he has been collaborating with researchers from the Open source Project for a Network Data Access Protocol (OPeNDAP) to develop a methodology for seamless merging of HF radar radial data from multiple distributed operators to produce current maps that can be provided via the internet.

Dr. Ullman is a member of the American Geophysical Union.



Eric Terrill received the B.E. degree from the Applied Mechanics and Engineering Sciences Department, University of California at San Diego, La Jolla, in 1993 and the Ph.D. degree in the applied ocean sciences from the Scripps Institution of Oceanography, University of California at San Diego, in 1998.

He is presently the Director of the Coastal Observing Research and Development Center at Scripps Institution of Oceanography. He is actively involved in the development and deployment of new observational techniques, sensor networks, and

observing platforms. He also manages a large scale array of HF radar systems that are being deployed in southern California. His research interests include coastal circulation, air-sea interaction, extreme storm events, water-quality, and naval hydromechanics. Sponsorship for his research activities is provided by the Office of Naval Research, the National Oceanic and Atmospheric Administration, the National Science Foundation, and the State of California.